NUCLEAR INSTRUMENTS AND METHODS 104 (1972) 317–332; © NORTH-HOLLAND PUBLISHING CO.

RESPONSE FUNCTIONS FOR SODIUM IODIDE SCINTILLATION DETECTORS*

M. J. BERGER and S. M. SELTZER

National Bureau of Standards, Washington, D.C. 20234, U.S.A.

Received 19 April 1972

The response of sodium iodide detectors to gamma rays has been calculated by a method that takes into account the multiple scattering and escape from the detector of the incident gamma rays as well as of the secondary charged particles and bremsstrahlung. The method is applicable to gamma rays with arbitrarily high energies, and its accuracy has been verified by comparisons with experimental response functions at energies up to 20 MeV. A systematic tabulation has been made of the response functions for $3'' \times 3''$ detectors irradiated with broad parallel beams of gamma rays, at energies between 100 keV and 20 MeV. These results are given in a parametrized form which makes it easy to interpolate with respect to incident gamma-ray energy. A few response functions have also been calculated for detectors irradiated with 50 MeV gamma rays. Exploratory calculations have shown that $3'' \times 3''$ detectors are "omnidirectional" in the sense that the shape of the response function depends very little on the direction of the incident gamma-ray beam. Therefore, the tabulated data for broad parallel beams incident perpendicularly can, in good approximation, also be applied to other source geometries, e.g. the case of a detector exposed to an isotropic gamma-ray flux.

1. Introduction

Increasingly complex and sophisticated methods are being used for the conversion of observed NaI pulse-height distributions into true gamma-ray spectra. These methods require accurate and detailed information about the detector response function which describes the stochastic relation between the pulse-heights and the energies of the incident gamma rays. The calculations reported here were undertaken in order to provide a reliable standard set of response functions as input for a conversion system developed by Trombka[1-3]) and his associates at Goddard Space Flight Center (NASA).

A large amount of experimental and calculated response function data has accumulated over the years. [For a good review, and references to the literature, see, e.g., Neiler and Bell[4]), and Van Lieshout et al.[5]).] The new contributions from our work are the following:

a. The loss of energy from the NaI detector due to the escape of secondary charged particles and bremsstrahlung is treated by a more detailed and realistic transport calculation than in previous work. This allows accurate determination of the response function for arbitrarily high energies of the incident gamma rays.

b. The validity of the calculations has been checked by numerous comparisons with experimental data, both old and recent, at energies up to 20 MeV.

c. A systematic tabulation has been made of the response functions for detectors with a commonly used size ($3'' \times 3''$) exposed to broad parallel beams of gamma rays. These results are given at 21 energies between 100 keV and 20 MeV, in a form which permits easy interpolation to any energy.

d. The dependence of the response function on the direction of the incident gamma-rays has been investigated.

* This work was carried out with the joint support of NASA and the Office of Naval Research.

2. Components of the response function

The *response function* $R(E_0,h)$ can be written as the convolution of an *energy deposition spectrum* $D(E_0,E)$ and a *resolution function* $G(E,h)$, multiplied by the *detection efficiency* $\eta(E_0)$:

$$R(E_0,h) = \eta(E_0) \int_0^{E_0} D(E_0,E)\, G(E,h)\, \mathrm{d}E. \qquad (1)$$

The various quantities in eq. (1) have the following meaning:

$R(E_0,h)\mathrm{d}h$ is the probability that a gamma ray incident with energy E_0 will give rise to a pulse with a height between h and $h+\mathrm{d}h$.

$\eta(E_0)$ is the probability that the incident gamma ray will have at least one interaction in the detector.

$D(E_0,E)\mathrm{d}E$ is the probability that the gamma ray, if it interacts with the detector at all, will deposit an amount of energy between E and $E+\mathrm{d}E$.

$G(E,h)\mathrm{d}h$ is the probability that the deposition of energy E will give rise to a pulse with a height between h and $h+\mathrm{d}h$.

The assumed normalization of the response function is such that the integral of $R(E_0,h)$ over all h is equal to

$\eta(E_0)$. The evaluation of the detection efficiency is a geometrical problem which has been solved analytically for various cases of interest[6-8]). The efficiency values from our Monte Carlo calculation were used primarily to check the correctness of our sampling procedures.

3. Calculation of the energy deposition spectrum

The calculation of $D(E_0,E)$ is a multiple scattering problem involving photons, electrons and positrons. The multiple Compton scattering of photons and their eventual escape from, or absorption in, the detector were simulated by random sampling, in direct analogy to the physical processes[9]). This was done for the incident gamma-rays as well as for all secondary photons (bremsstrahlung, annihilation quanta, fluorescence radiation), using cross sections for Compton scattering, photoelectric absorption and pair production taken from a compilation by Hubbell[10]). The multiple scattering of the electrons and positrons set in motion in gamma-ray interactions (photoelectrons, Compton electrons, electron–positron pairs) was treated by a Monte Carlo model in which, instead of sampling all successive interactions, the combined effect of many successive scattering was taken into account with the use of analytical multiple-scattering theory[11]). Each electron track to be simulated was divided into many short segments; the multiple-scattering angular deflection in each segment was sampled from the Goudsmit–Saunderson[12]) distribution, and the energy loss from the Landau[13]) distribution. In each path segment the electron was given a chance to set in motion secondary (knock-on) electrons in inelastic collisions [according to the Møller[14]) cross section], to produce characteristic X-rays via K-shell ionization [according to the Kolbenstvedt[15]) cross section], and to emit bremsstrahlung [according to a combination of Born-approximation cross sections with semi-empirical corrections described elsewhere[16])]. Positrons were treated as if they were electrons, except that the emission of annihilation quanta (from positrons at rest) was allowed to occur.

Monte Carlo histories were terminated when the electron or photon escaped from the detector or when its energy dropped to a value below 10 keV. Electron histories were also terminated when the energy of the electron fell to a value smaller than 4% of the incident gamma-ray energy, provided this took place deep enough in the detector so that the residual electron range was smaller than the distance to the nearest detector boundary*. All energy remaining upon termination of a Monte Carlo history was considered to have been deposited in the detector. Because of the 10 keV cut-off, only fluorescence radiation from the K-shell of iodine had to be included.

For each sampled Monte Carlo cascade, consisting of the history of the incident gamma ray and the histories of all secondary photons and charged particles, the energy E deposited in the detector was scored as the difference between the incident gamma-ray energy E_0 and the sum of the energies carried away by escaping electrons, positrons or photons. By sampling large numbers of such cascades (typically 10000 to 50000), estimates of the energy deposition spectrum were obtained. This spectrum has the form of a line spectrum plus a continuum $C(E_0,E)$:

$$D(E_0,E)=C(E_0,E)+P_0\delta(E-E_0)+P_1\delta(E-E_0+mc^2)+P_2\delta(E-E_0+2mc^2)+P_3\delta(E-\bar{E}_f), \quad (2)$$

where δ is the delta function and mc^2 the electron rest energy. P_0 is the probability that the entire gamma-ray energy E_0 is deposited in the detector. P_1 and P_2 are the probabilities that all of the energy is deposited with the exception of the amounts mc^2 or $2mc^2$ carried away by one or two unscattered annihilation quanta. P_3 is the probability that all energy is deposited except that carried away by unscattered K X-rays from iodine (with a weighted average energy $\bar{E}_f=29$ keV)†. The quantity P_0 can also be interpreted as the relative area under the *total absorption peak* of the response function. Similarly, P_1 and P_2 are the relative areas under the *single* and *double annihilation radiation escape peaks*, and P_3 is the relative area under the *fluorescence radiation escape peak*.

The computation of gamma-ray Monte Carlo histories was relatively fast. Neglecting secondary electrons, only ≈ 0.5 min of time on an IBM 360/91 computer was needed to trace the histories of 10000 gamma rays incident on a $3''\times 3''$ detector. The cost of tracing electron Monte Carlo histories was much higher. For example, with the inclusion of all charged-particle and bremsstrahlung secondaries, the time required to follow the cascades generated by 10000 gamma rays incident on a $3''\times 3''$ detector was ≈ 5 min for an

* This cut-off procedure greatly speeded up the calculation, but resulted in a slight underestimate of the bremstrahlung emitted by low-energy electrons. From the examination of tabulated bremsstrahlung efficiency values (ref. 17) and from trial calculations with different cut-off procedures, we reached the conclusion that the effect of the adopted cut-off procedure on the calculated energy deposition spectra was negligible.

† Actually the computer program gives information about individual escape peaks associated with the escape of K_{α_1}, K_{α_2}, K_{β_1} and K_{β_2} quanta whose energies are 28.612, 28.317, 32.295 and 33.047 keV, and whose relative intensities are 0.542, 0.279, 0.148 and 0.031, respectively.

TABLE 1
Values of the exponent n in eq. (4) for the detector resolution, derived from various sets of experimental data.

Author	Energy	n
Trombka[a]	0.279 MeV to 2.76 MeV	0.32
Trombka[b]	0.032 MeV to 2.76 MeV	0.34
Ferguson et al.[c]	0.030 MeV to 1.332 MeV	0.34
Steyn[d]	0.073 MeV to 2.754 MeV	0.375
McGowan[e]	0.081 MeV to 1.850 MeV	0.33

[a] Priv. comm; analysis of expt. data obtained at Goddard SFC.
[b] Priv. comm; analysis of expt. data of Heath (ref. 19).
[c] Priv. comm; analysis of data obtained at Howard University.
[d] Ref. 18.
[e] Our least-squares analysis of McGowan's data from Oak Ridge National Laboratory as reported by Kelley et al. [20]).

incident gamma-ray energy of 2 MeV, ≈12 min at 20 MeV and ≈24 min at 50 MeV.

4. Determination of the resolution function

It is well known that the resolution function $G(E,h)$ can be closely approximated by a Gaussian whose mean value $\bar{h}$ is proportional* to E and whose standard deviation $\sigma(E)$ must be obtained from experimental data. The *resolution* of the detector is defined to be the ratio

$$r(E) = 100\ W(E)/E \text{ (percent)}, \qquad (3)$$

where $W = 2\sigma\sqrt{(2\log 2)}$ is the full width at half maximum of the Gaussian. The energy dependence of the detector resolution can be expressed by a power law,

$$r(E) = r(E')(E'/E)^n, \qquad (4)$$

where E' is a reference energy which – in agreement with common usage – we take to be the energy of ^{137}Cs gamma rays (0.661 MeV). As discussed later in section 8, the magnitude of $r(0.661)$ typically ranges from 7% to 12%.

On the basis of simple statistical arguments it has often been assumed that the power n in eq. (4) has the value $\frac{1}{2}$. However, a better fit to the experimental data can be obtained with $n \approx \frac{1}{3}$, as pointed out by Trombka and Adler[3]) and Steyn[18]). Table 1 summarizes various analyses of experimental data, by Trombka [using his own data as well as those of Heath[19])], by Ferguson (priv. comm.), by Steyn[18]) and by Kelley et al.[20]). These analyses have led us to adopt in our work the value $n = 0.34$.

* The proportionality applies provided that a possible non-linearity of channel number versus energy has been removed by an appropriate correction [see, e.g. Heath[19])].

5. Some comparisons at low energies

Even though this paper is focussed mainly on the response function at high energies, it is well to begin by making a few comparisons at low energies where charged-particle motion and escape are unimportant.

Various authors have calculated, at energies from 10 to 100 keV, the ratio of the fluorescence escape peak to the total absorption peak, P_3/P_0. At 100 keV, for the case of perpendicular incidence on a large detector, an approximate analytical calculation by Axel[21]) gave the value 0.04, a similar calculation by Fioratti and Piermattei[22]) the value 0.0365, a Monte Carlo calculation by Israel et al.[23]) the value 0.042, and the present work the value 0.040. These results are on the whole consistent with each other, and have been shown by Fioratti and Piermattei to be in approximate agreement with the experimental data. Heath[19]) obtained the experimental value 0.056 for a 3″ × 3″ detector.

We now turn to the comparison of calculated and experimental values of the total absorption peak, P_0, at an energy of 0.661 MeV. Table 2 contains comparisons, for the case of a narrow pencil beam, between results of our program [using cross sections from Hubbell[10]) and from an earlier tabulation by Grodstein[24])], previous calculated values of Berger and Doggett[25]) and Miller and Snow[26]), and experimental values of Jarczyk et al.[27]), Schmidt[28]) and Foote and Koch[29]). In table 3, comparisons are made, for the case of a broad parallel beam, between our results, the calculations of Miller and Snow[26]) and Giannini et al.[30]), and experimental values of Jarczyk et al.[27]). The following conclusions can be drawn from these comparisons:

a. The agreement between the various calculations is, by and large, satisfactory.

TABLE 2
Comparison of calculated and experimental values of the total absorption peak, P_0, for detectors irradiated with a narrow pencil beam of 0.661-MeV gamma rays.

Detector size	Calculated				Experimental		
	This work[a]	This work[b]	Berger and Doggett[25])	Miller and Snow[26])	Jarzcyck et al.[27])	Schmidt[28])	Foote and Koch[29])
1″ × 1″	0.384	0.367	0.377				
2″ × 2″	0.574	0.559			0.51		
3″ × 3″	0.703	0.689			0.65		
4″ × 4″	0.790	0.779					
5″ × 4″	0.818	0.808	0.821	0.819	0.74	0.71	0.8

[a] Using gamma-ray cross sections from Hubbell[10]). [b] Using gamma-ray cross sections from Grodstein[24]).

TABLE 3
Comparison of calculated and experimental values of the total absorption peak, P_0, for detectors irradiated with a broad parallel beam of 0.661-MeV gamma rays.

Detector size	Calculated			Experimental
	This work	Miller and Snow[26])	Giannini et al.[30])	Jarczyk et al.[27])
2″ × 2″	0.478	0.470	0.461	0.40
3″ × 3″	0.569			0.50
4″ × 4″	0.664	0.652		
5″ × 4″	0.698			0.58

b. In the cases examined, the change in the value of P_0 resulting from the use of different cross sections ranges from 1.2% for large detectors to 4.5% for small detectors*.

c. The experimental values of P_0 tend to be significantly lower than the calculated values, by as much as 10–20%.

These discrepancies are most probably due to the fact that the calculations were done for an idealized bare detector and failed to take into account the scattering (and backscattering) of radiation into the detector from surrounding material. Some Monte Carlo calculations have already been made by Nardi[31]) and Steyn et al.[32]) that include the effects of gamma-ray scattering in the cladding material around the NaI crystals and in the photomultiplier tube. Nardi has also demonstrated that there are additional perturbations of the response function which must be due to scattered gamma-rays from other pieces of equipment, walls, etc. Still to be done are high-energy response function calculations which include the effects of the scattering (and backscattering) of secondary electrons in surrounding materials.

* The differences, although small, are statistically significant. They are based on samples of 10000 histories, calculated twice with different cross sections, but using the same sequence of random numbers.

6. Effect of charged-particle and bremsstrahlung escape on the response function

In order to explore the effect of the escape of electrons, positrons and bremsstrahlung, we have carried out response-function calculations not only with the complete Monte Carlo model but also with a simplified model in which these effects were omitted. A typical comparison of the results obtained with the two models is given in fig. 1, for the case of a narrow pencil beam of 10.83 MeV electrons incident on a 3″ × 3″ detector. Use of the simplified model results in a considerable overestimate of the total absorption peak and the first and second annihilation radiation escape peaks, and a corresponding underestimate of the low-pulse-height tail of the response function. Fig. 2 compares the peak parameters P_0, P_1, P_2 and P_3 obtained with the two Monte Carlo models for gamma-rays with energies between 100 keV and 20 MeV incident on a 3″ × 3″ detector. The differences begin to be noticeable at 3 MeV where they amount to $\approx 10\%$,

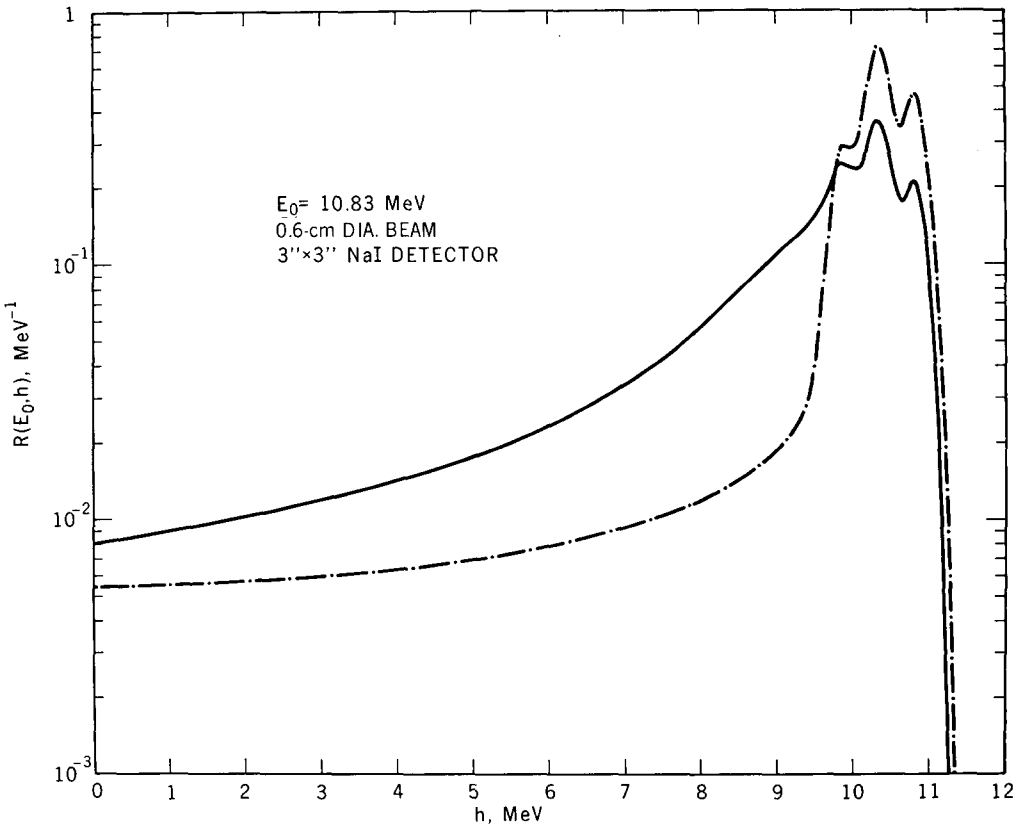

Fig. 1. Effect on the response function of the escape of bremsstrahlung and charged particles from the detector. Dashed curve was calculated with omission of these effects.

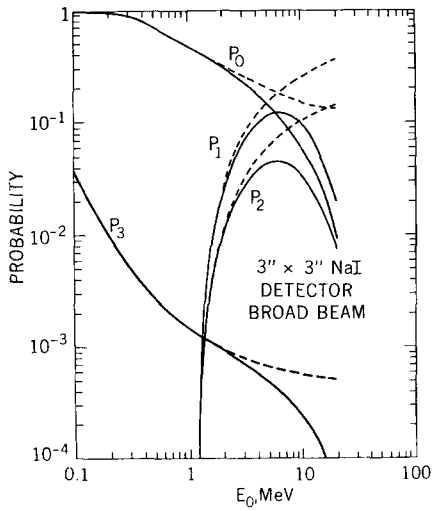

Fig. 2. Total absorption peak (P_0), single and double annihilation radiation escape peaks (P_1 and P_2) and iodine K-shell fluorescence escape peak (P_3). Dashed curves are calculated disregarding the escape of bremsstrahlung and secondary charged particles.

and then rapidly increase at higher energies. The correct values of P_1 and P_2 reach a peak at 5 MeV and rapidly decrease at higher energies, whereas the results from the simplified model continue to rise. The effects of charged-particle and bremsstrahlung escape are clearly important enough to justify the computational effort that goes into the calculation of electron transport.

7. Comparisons with previous high-energy calculations

Various approximations have been used in the past to calculate charged-particle and bremsstrahlung escape from sodium iodide detectors. Zerby and Moran[33]) evaluated the spectrum of the bremsstrahlung emitted by an electron in the course of being slowed down to rest in an unbounded sodium iodide medium. They used the continuous-slowing-down approximation and assumed the radiative energy loss to be small compared to the collision energy loss. The Zerby–Moran spectrum was used in response-function calculations by Zerby and Moran[34]), Miller and Snow[26]), and Weitkamp[35]).

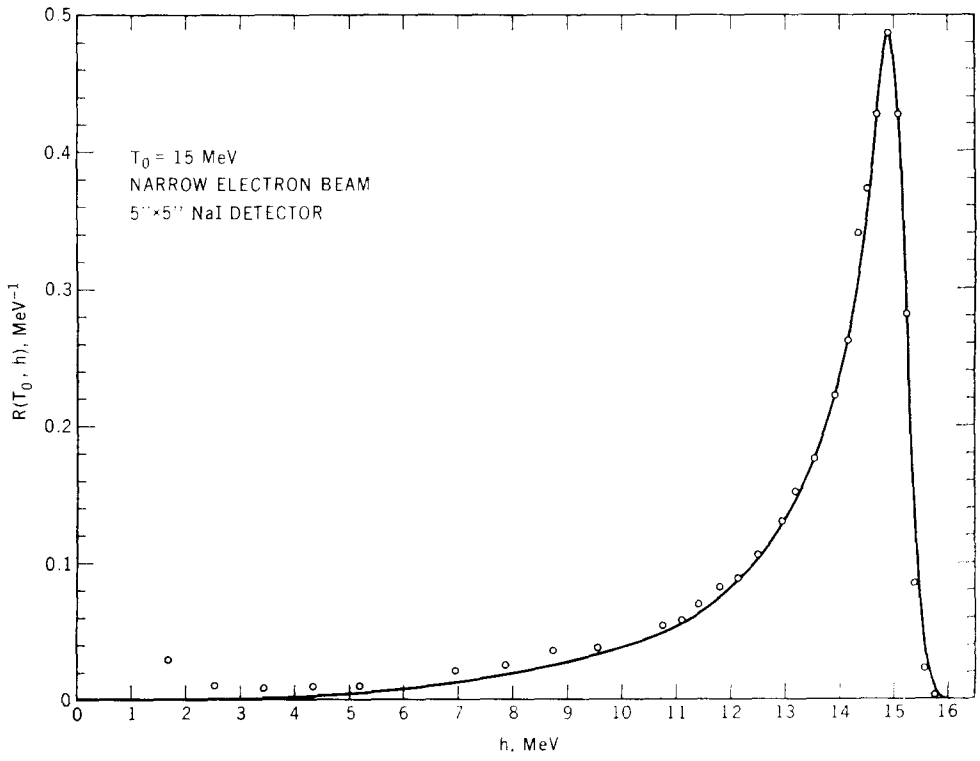

Fig. 3. Experimental response function of Koch and Wyckoff (points), and corresponding Monte Carlo result (curve), for a beam of 15 MeV electrons incident on a $5'' \times 5''$ detector. The experimental beam spread was approximated in the calculation by assuming a uniform beam with a 2 cm diameter. Assumed resolution $r(0.661) = 12\%$.

Zerby and Moran neglected electron motion altogether. Miller and Snow assumed the electrons to travel in a straight line, through a distance equal to the electron range. Giannini et al.[30]) made two improvements: they used a more accurate bremsstrahlung spectrum, derived without the assumption that the radiative loss is relatively small; they improved the treatment of electron transport through use of a Monte Carlo model introduced by Wilson[36]) which assumes initial straight-line travel followed by terminal diffusion.

In the present calculation the electron paths were divided into many segments whose length was chosen so that the average energy decrease per segment was 5%. The energy loss sampled for each segment took into account energy-loss straggling. The change of electron energy and direction was traced from segment to segment. This provided the basis for an accurate estimate of electron escape form the detector, and for the accurate evaluation of the angular and energy distribution of the bremsstrahlung emitted in the detector.

The validity of the method used for the calculation of electron and bremsstrahlung transport has been confirmed in various ways. Good agreement has been obtained in comparisons with the following experimental results: (a) the response of silicon detectors to electrons with energies up to 1 MeV[37]); (b) the backscattering of 1 MeV electrons from a large NaI detector, as measured by Titus[38]); (c) the emission of bremsstrahlung from a thick tungsten target as measured by O'Dell et al.[16,39]); (d) the response of a $5'' \times 5''$ NaI detector to 15 MeV electrons as measured by Koch and Wyckoff[40]), this comparison is shown in fig. 3.

Figs. 4a and b compare energy deposition spectra obtained by Miller and Snow[26]) at 8 MeV, and by Giannini et al.[30]) at 12 MeV, with our results. The low-energy part of our spectrum is considerably higher than that of Miller and Snow, and somewhat higher than that of Giannini. Comparisons of the total absorption peaks and first and second annihilation escape peaks are given in table 4. The Miller–Snow values for P_0, P_1 and P_2 exceed ours by 38%, 37% and 81%, respectively. The Giannini values for P_0 and P_1 are about the same as ours, but their P_2-value is 52% higher.

The Miller–Snow and Giannini results are based on Monte Carlo samples of 10000 gamma-rays with at least one interaction in the detector, and ours on a sample of 10000 incident gamma rays. The differences between the results from the different calculations are several times larger than the statistical uncertainties, and are presumably due to the differences in the Monte Carlo models. The trend of the discrepancies is not unexpected. Inasmuch as the energy deposition spectra under discussion pertain to a broad parallel beam

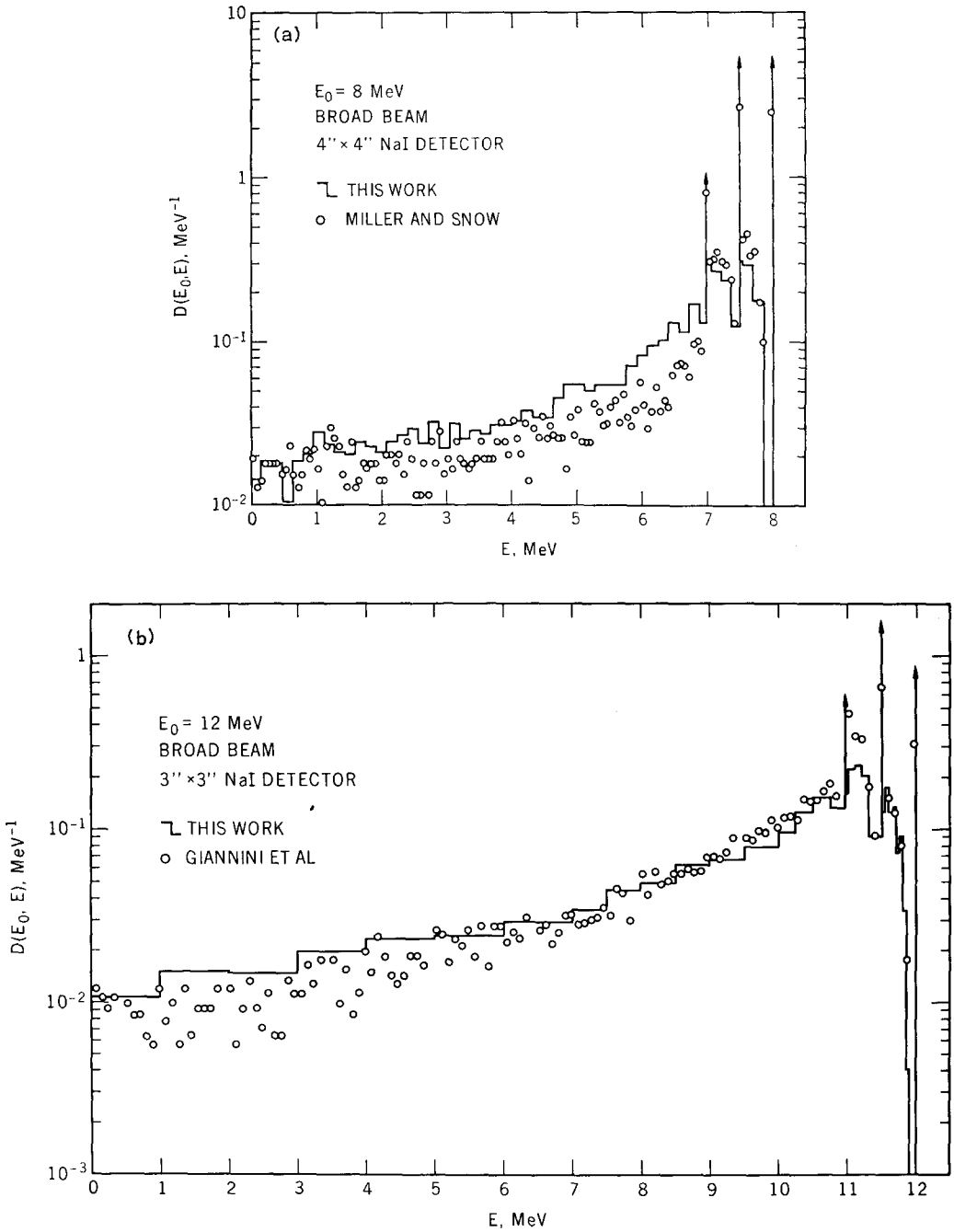

Fig. 4. Energy deposition spectra from different calculations. Arrows indicate positions of the total absorption peak and of the single and double annihilation radiation escape peaks. Areas under these peaks are given in table 4. a) Comparison with Monte Carlo calculation of Miller and Snow[26]). b) Comparison with Monte Carlo calculation of Giannini et al.[30]).

TABLE 4
Comparison of various calculated results for the total absorption peak (P_0) and the single and double annihilation radiation escape peaks (P_1 and P_2). The data apply to broad parallel beams.

		P_0	P_1	P_2
Source energy 8 MeV				
4″ × 4″ detector	Miller and Snow	0.192	(0.194)	(0.0491)
	This work	0.139	0.142	0.0270
Source energy 12 MeV				
3″ × 3″ detector	Giannini et al.	0.0425	(0.0755)	(0.0402)
	This work	0.0414	0.0753	0.0276

Entries in parentheses were obtained by subtracting the continuum contribution from the tabulated $D(E_0,E)$-histogram.

TABLE 5
Detector resolution $r(0.661)$, as defined by eq. (4), for various source-detector combinations for which experimental and calculated response functions are compared in figs. 5–7.

Figure	Experimenter	$r(0.661)$ (percent)	Method of determination
5a,b	Heath[19])	8.3	Measured at 0.661 MeV
5c	Lazar[41])	8.5	Measured at 0.479 MeV
6a	Metzger (priv. comm.)	7.3	Measured at 0.661 MeV
6b	Trombka et al.[42])	7.4	Measured at 0.661 MeV
6c	Jarczyk et al.[27])	7.7	Through comparison of expt. and calc. response functions in fig. 6c
7	Kockum and Starfelt[43])	11.5	Measured at 1.28 MeV

incident perpendicularly, the secondary electrons and bremsstrahlung would penetrate straight into the detector if it were not for multiple scattering. When the assumption of straight-line motion is replaced by a more realistic transport treatment, the chance of energy escape through the lateral surface of the detector is enhanced, and the absorption and escape peaks are lowered.

8. Comparisons with high-energy experiments

At energies above 3 MeV the experimental determination of NaI detector response functions becomes increasingly difficult because monoenergetic sources are lacking and background problems are usually severe. High-quality experimental data have been obtained in a limited number of cases; however, interpolation in these data with respect to incident gamma-ray energy is hardly feasible. It appears to be most advantageous to use the available experimental data to check the validity of calculational methods, and then to rely on systematic computations for the production of extensive response function libraries.

At high energies it is hard to determine the values of P_0, P_1 and P_2 by measuring the areas under the peaks of the experimental response functions, because the

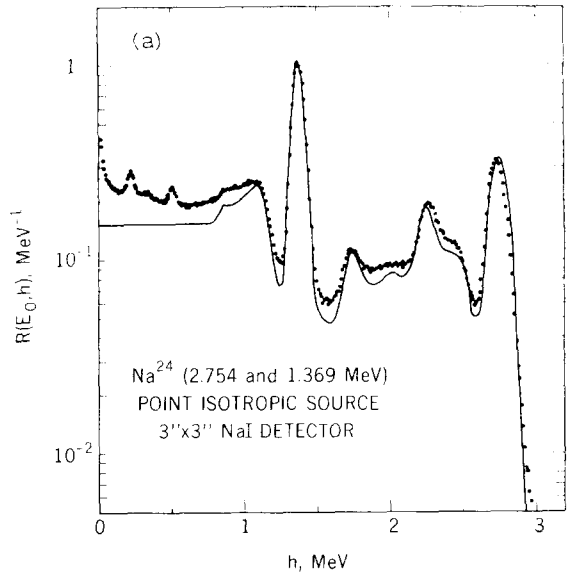

width of the Gaussian resolution function is not small compared to the separation of the peak energies. Comparisons with calculated results are therefore best made for the response function itself in the peak region.

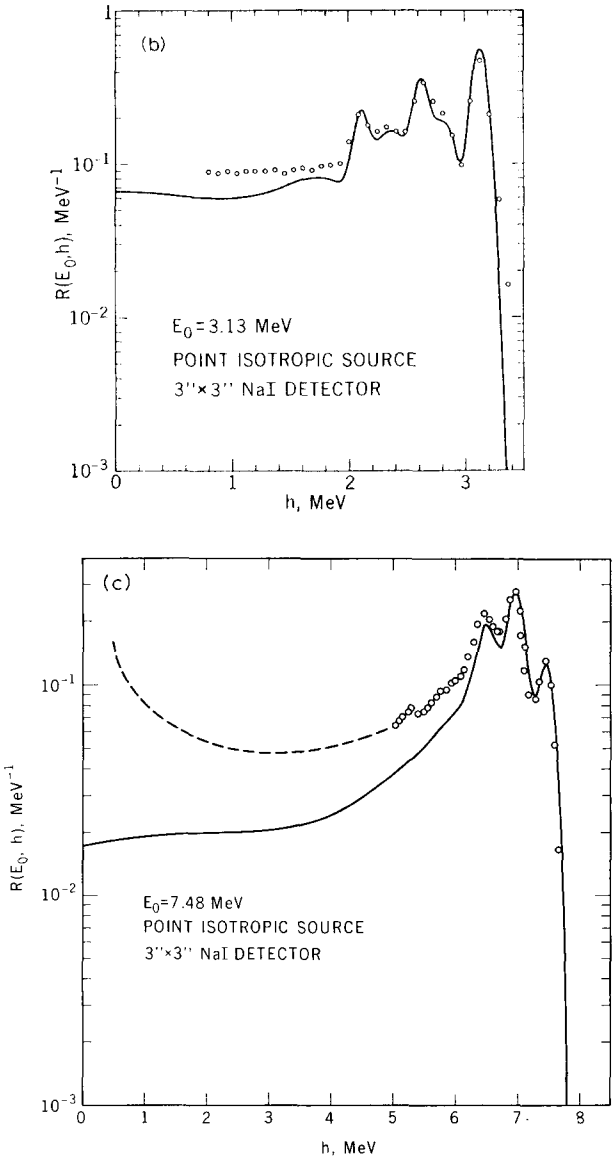

Fig. 5. Response functions for detectors irradiated with gamma rays from point-isotropic sources. Points are experimental and curves are calculated. a) Comparison with an experimental response function obtained by Heath[19]) with a radioactive ^{24}Na source at a distance of 10 cm from the detector. b) Comparison with an experimental response function obtained by Heath[19]) with a radioactive ^{37}S source at a distance of 10 cm from the detector. c) Comparison with an experimental response function obtained by Lazar with a ^{9}Be(p,γ) source at a distance of 9.3 cm from the detector. Dashed curve represents experimental data in region of very high background.

The values of the experimental detector resolution $r(0.661)$ used in the comparisons are listed in table 5. The calculated response functions are normalized to one incident gamma-ray photon, so that the area under each curve is equal to the detection efficiency. The experimental data are usually presented as relative number of counts versus channel number. We have renormalized them so as to obtain the best agreement with the calculated response function in the pulse-height region including the total absorption and first and second escape peaks.

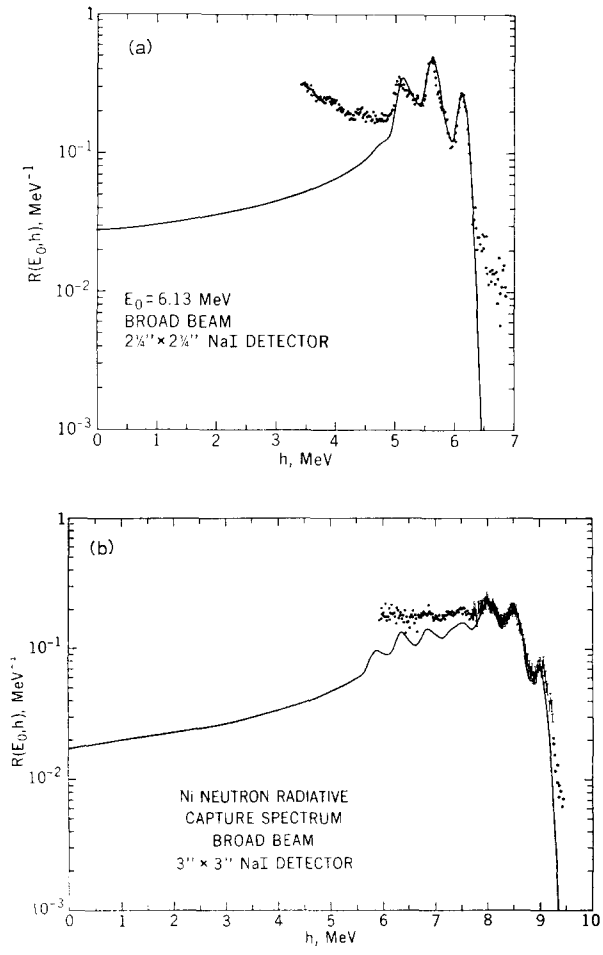

Fig. 6. Response functions for detectors irradiated by broad parallel beams. Points are experimental and curves calculated. a) Comparison with an experimental response function obtained by Metzger (private communication) with a ^{244}Cm/^{13}C (α,γ) source. b) Comparison with an experimental response function obtained by Trombka with gamma rays from radiative capture of thermal neutrons in Ni. The calculation takes into account the following five most prominent lines of the gamma-ray spectrum: 8.999, 8.533, 7.819, 7.536 and 6.837 MeV, for which the numbers of photons/100 neutrons are, respectively: 41.65, 18.74, 9.04, 4.93, 11.91.

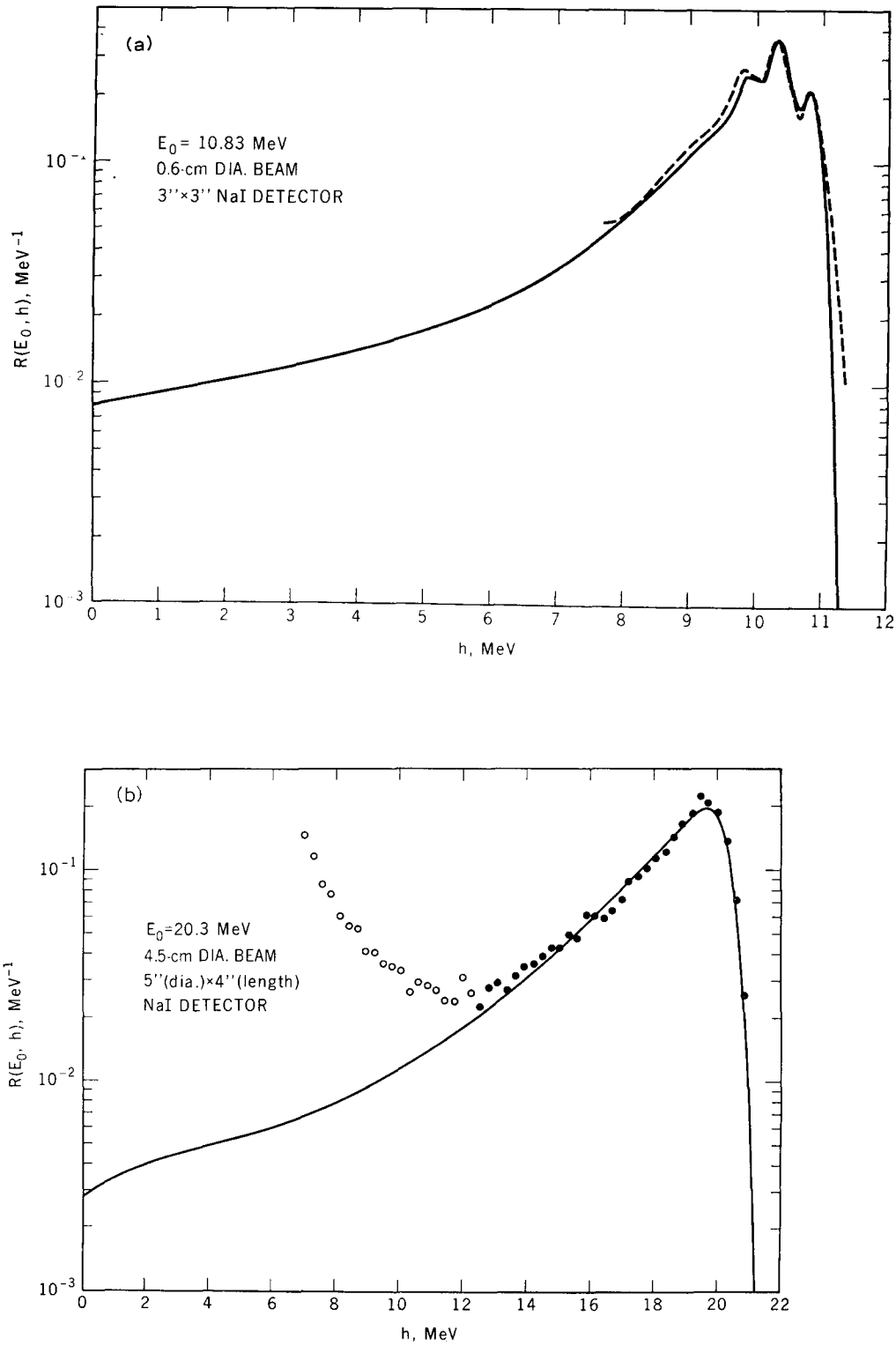

Fig. 7. Response functions for detectors irradiated by narrow beams. a) Comparison with an experimental response function (dashed curve) obtained by Jarczyck et al.[27]) with a $^{14}N(n,\gamma)$ source. b) Comparison with an experimental response function (points) obtained by Kockum and Starfelt[43]) with a $^{3}H(p,\gamma)$ source.

Figs. 5a, b and c show comparisons with experimental results of Heath[19]) and Lazar[41]) for point-isotropic gamma-ray sources located on the detector axis. Figs. 6a and b show comparisons with results of Metzger (private communication) and Trombka et al.[42]) obtained with broad parallel beams.

Figs. 7a and b show comparisons with results obtained by Jarzcyck et al.[27]) and by Kockum and Starfelt[42]) with narrow beams. The various experiments cover incident gamma-ray energies between 3 MeV and 20 MeV.

The trends indicated by the various comparisons are rather similar. There is good agreement between calculated and experimental results in the upper third of the pulse-height distribution, a region which includes the total absorption peak and the first and second annihilation radiation escape peaks. At pulse heights below this region the experimental response functions typically exhibit a rise, often rather steep, to values that greatly exceed the theoretical values*. Kockum and Starfelt explained this rise in their data as due to background from neutron and gamma-ray contamination. Similarly, Jarzcyk et al. reported their response functions only in the region of large pulse heights, because of the strong background at lower pulse heights.

* By contrast, there is good agreement between experiment and calculation for the electron response function measured by Koch and Wyckoff at 15 MeV, as shown in fig. 3. In this case, with an electron beam as radiation source, the background problem was minimal.

In the absence of techniques for eliminating such background it will remain necessary to rely on calculations for the lower two-thirds of the pulse-height distribution.

9. Response functions at 50 MeV

Response functions for incident gamma-ray energies above 20 MeV are of potential interest for a number of applications. It has been shown by Hofstadter and coworkers[44,45]) that very large NaI crystals can be successfully used as total absorption spectrometers for electrons and photons in the energy range of 0.1 to 15 GeV. At more moderate energies, monoenergetic gamma-ray beams with energies of 30 to 40 MeV are coming into use[46]), in experimental arrangements that utilize the annihilation of positrons in flight. In gamma-ray astronomy the occurrence of gamma-ray fluxes with energies up to 50 MeV or higher has been reported[48-50]). We have made a few exploratory calculations of response functions at 50 MeV, for detector sizes that appear to be readily available commercially. The results are shown in fig. 8.

10. Response function tabulations

The most commonly used NaI detector for single-crystal gamma-ray spectroscopy is the 3″ × 3″ detector. We now present data from which one can easily construct the response function for such a detector, for incident gamma-ray energies between 100 keV and 20 MeV. The results are for a broad parallel beam

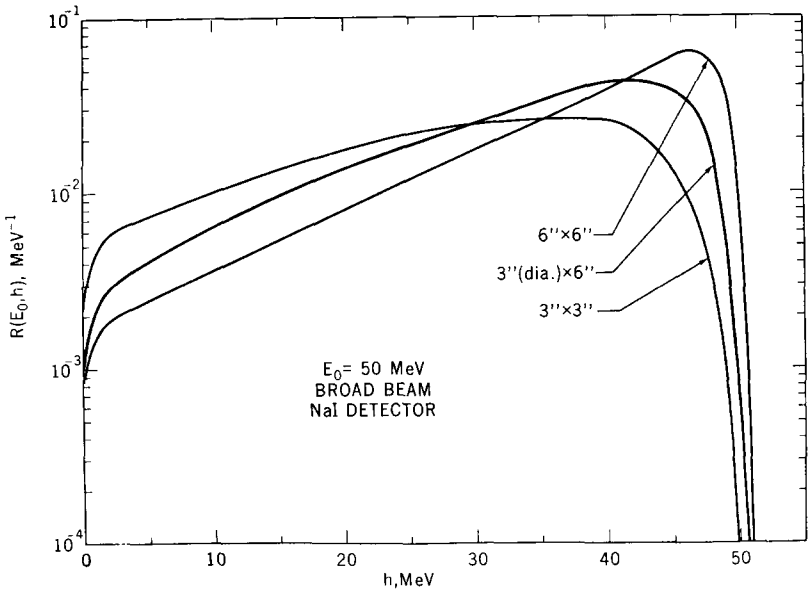

Fig. 8. Calculated response functions for detectors irradiated with broad parallel beams of 50 MeV gamma rays. Assumed detector resolution is $r(0.661) = 7.5\%$.

TABLE 6
Calculated values of the total absorption peak, P_0, single and double annihilation radiation escape peaks, P_1 and P_2, and the iodine K-shell fluorescence radiation escape peak, P_3. Results pertain to broad parallel beams incident perpendicularly on the endface of a $3'' \times 3''$ detector.

E_0 (MeV)	P_0	P_3	E_0 (MeV)	P_0	P_1	P_2
0.1	0.958	0.0382	1.2	0.425	0.00005	0.00007
0.15	0.963	0.0169	1.5	0.370	0.0056	0.0025
0.2	0.946	0.0101	2.0	0.304	0.0234	0.0099
0.3	0.875	0.0055	3.0	0.225	0.0643	0.0257
0.4	0.779	0.0038	4.0	0.178	0.0979	0.0366
0.5	0.697	0.0029	5.0	0.143	0.114	0.0425
0.6	0.627	0.0024	6.0	0.117	0.119	0.0446
0.8	0.534	0.0019	8.0	0.0793	0.112	0.0419
1.0	0.471	0.0016	10.0	0.0567	0.0951	0.0327
1.2	0.425	0.0014	12.0	0.0425	0.0720	0.0248
			15.0	0.0259	0.0444	0.0161
			20.0	0.0092	0.0198	0.0074

incident on the flat endface of a cylindrical detector. As will be discussed in section 11, $3'' \times 3''$ detectors are sufficiently symmetric so that the response function (divided by the detection efficiency), $R(E_0,h)/\eta(E_0)$, is rather independent of the directional distribution of the incident gamma-ray beam. The tabulated results can therefore be applied, at least approximately, to various other beam geometries of interest, for example the case of an isotropic gamma-ray flux that may be of interest in gamma-ray astronomy.

Monte Carlo calculations of the energy deposition spectrum $D(E_0,E)$ have been carried out for 20 values of E_0 between 100 keV and 20 MeV, in each case with a sample of 50000 incident gamma rays. The resulting values of the peak parameters P_0, P_1 and P_2 (and the values of P_3 at energies up to 1.2 MeV) are given in table 6. The standard deviation of P_k is

$$[P_k(1-P_k)/50000]^{\frac{1}{2}}.$$

We have found it advantageous to express the continuous part of the energy deposition spectrum, $C(E_0,E)$, in terms of dimensionless functions C_j, $(j=1,2,3,4)$ which depend on dimensionless energy-related variables x, y and z. The representation of the data has been arranged so as to minimize the explicit dependence on E_0, and to facilitate interpolation with respect to E_0 and E.

For $E_0 \leqq 1.2$ MeV, we set

$$C(E_0,E) = C_1(E_0,x)(1+mc^2/2E_0)/E_0, \tag{5}$$

where

$$x = E(1+mc^2/2E_0)/E_0. \tag{6}$$

For $E_0 > 1.2$ MeV, we set

$$C(E_0,E) = C_2(E_0,y)/(E_0-2mc^2), \quad \text{for } 0 \leqq E < E_0-2mc^2, \tag{7a}$$

$$C(E_0,E) = C_3(E_0,z)/2mc^2, \quad \text{for } E_0-2mc^2 \leqq E < E_0-mc^2, \tag{7b}$$

$$C(E_0,E) = C_4(E_0,z)/2mc^2, \quad \text{for } E_0-mc^2 \leqq E \leqq E_0, \tag{7c}$$

where

$$y = E/(E_0-2mc^2) \tag{8}$$

and

$$z = (E-E_0+2mc^2)/2mc^2. \tag{9}$$

The functions C_j are given in table 7. By comparing the results of different Monte Carlo runs, and by examining the dispersion of the data prior to smoothing, we arrived at the estimate that the statistical error (relative standard deviation) of most of the $C(E_0,E)$-values is approximately 5, 8, 11 and 13% for $E_0 = 1,6$, 12 and 20 MeV, respectively. The estimated statistical accuracy of the response functions obtained with the use of the data in tables 6 and 7 is 3% or better in the peak region, and 5–15% in the continuum region.

We have developed a spline interpolation program, utilizing an algorithm given by Ahlberg et al.[51]), in order to construct the response function from the tabulated data. The program performs a simple interpolation with respect to E_0 in table 6, and a double interpolation, with respect to E_0 and x, y or z, on the data in table 7. Finally, the program convolutes the energy deposition spectrum with a Gaussian resolution function according to eq. (1). A family of response functions generated in this manner for $E_0 =$ 2, 3, 4, ⋯, 20 MeV is shown in fig. 9.

TABLE 7

Calculated values of the continuous part of the energy deposition spectrum, for broad parallel beams incident perpendicularly on the endface of a 3″ × 3″ detector.

E_0 (MeV)	0.10	0.15	0.20	0.30	0.40	0.50	0.60	0.80	1.00	1.20
x					$C_1(E_0,x)$					
0.00	0.00000	0.00000	0.00062	0.0403	0.128	0.200	0.255	0.323	0.359	0.373
0.05	0.00045	0.00615	0.0202	0.0835	0.176	0.252	0.304	0.359	0.390	0.411
0.10	0.00090	0.00870	0.0259	0.0940	0.191	0.270	0.320	0.372	0.401	0.421
0.20	0.00181	0.0105	0.0314	0.112	0.206	0.281	0.336	0.390	0.414	0.429
0.30	0.00142	0.00960	0.0310	0.114	0.213	0.291	0.348	0.410	0.435	0.446
0.40	0.00057	0.00790	0.0272	0.108	0.209	0.294	0.358	0.418	0.451	0.467
0.50	0.00069	0.00735	0.0260	0.0970	0.200	0.290	0.355	0.427	0.470	0.495
0.60	0.00220	0.00855	0.0226	0.0880	0.190	0.279	0.352	0.442	0.497	0.530
0.70	0.00975	0.0193	0.0350	0.0940	0.183	0.269	0.347	0.459	0.530	0.583
0.80	0.0168	0.0280	0.0502	0.120	0.201	0.280	0.357	0.496	0.597	0.677
0.90	0.0238	0.0505	0.0855	0.166	0.254	0.345	0.433	0.591	0.720	0.820
0.95	0.0280	0.0635	0.105	0.193	0.294	0.391	0.485	0.653	0.795	0.917
0.975	0.0310	0.0707	0.113	0.207	0.308	0.408	0.507	0.680	0.835	0.970
1.00	0.0115	0.0165	0.0230	0.0440	0.0880	0.177	0.266	0.435	0.523	0.597
1.10	0.00051	0.00183	0.00412	0.0118	0.0228	0.0299	0.0330	0.0303	0.0237	0.0164
1.20	0.00003	0.00075	0.00188	0.00315	0.00338	0.00288	0.00151	0.00001	0.00000	0.00000

E_0 (MeV)	1.2	1.5	2.0	3.0	4.0	5.0	6.0	8.0	10.0	12.0	15.0	20.0
y					$C_2(E_0,y)$							
0.00	0.0672	0.155	0.238	0.276	0.269	0.246	0.229	0.200	0.178	0.155	0.132	0.118
0.05	0.0715	0.163	0.240	0.276	0.271	0.247	0.231	0.213	0.204	0.199	0.194	0.197
0.10	0.0728	0.166	0.241	0.277	0.272	0.248	0.233	0.222	0.220	0.226	0.238	0.260
0.20	0.0735	0.167	0.242	0.278	0.275	0.252	0.243	0.243	0.251	0.265	0.297	0.326
0.30	0.0740	0.168	0.243	0.279	0.282	0.265	0.260	0.267	0.283	0.303	0.334	0.390
0.40	0.0744	0.169	0.245	0.289	0.300	0.290	0.286	0.300	0.323	0.351	0.400	0.490
0.50	0.0752	0.170	0.247	0.298	0.319	0.319	0.322	0.350	0.387	0.430	0.497	0.625
0.60	0.0757	0.171	0.257	0.317	0.348	0.364	0.377	0.416	0.473	0.535	0.634	0.810
0.70	0.0760	0.172	0.268	0.340	0.385	0.422	0.455	0.515	0.597	0.697	0.843	1.09
0.80	0.0767	0.173	0.279	0.378	0.431	0.492	0.556	0.692	0.830	0.975	1.18	1.51
0.90	0.0774	0.174	0.297	0.419	0.527	0.657	0.795	1.16	1.35	1.59	1.90	2.15
0.95	0.0777	0.175	0.303	0.438	0.590	0.780	1.00	1.47	1.94	2.29	2.57	2.54
0.975	0.0779	0.175	0.307	0.452	0.605	0.790	1.02	1.54	2.11	2.60	2.90	2.68
1.00	0.0780	0.175	0.309	0.466	0.614	0.785	1.00	1.47	1.94	2.18	2.19	1.90
z					$C_3(E_0,z)$							
0.00	0.450	0.373	0.347	0.350	0.388	0.430	0.451	0.439	0.402	0.351	0.261	0.128
0.10	0.460	0.399	0.363	0.370	0.396	0.430	0.451	0.439	0.391	0.339	0.253	0.138
0.20	0.478	0.424	0.388	0.381	0.397	0.412	0.427	0.417	0.374	0.325	0.247	0.124
0.30	0.501	0.464	0.423	0.388	0.376	0.375	0.376	0.356	0.309	0.260	0.189	0.0899
0.35	0.519	0.485	0.437	0.380	0.344	0.319	0.298	0.262	0.222	0.180	0.128	0.0690
0.40	0.542	0.502	0.455	0.378	0.320	0.276	0.241	0.192	0.157	0.127	0.0910	0.0496
0.45	0.574	0.521	0.461	0.370	0.305	0.259	0.223	0.171	0.134	0.107	0.0756	0.0406
0.50	0.603	0.542	0.467	0.368	0.304	0.258	0.222	0.168	0.129	0.0986	0.0675	0.0371
z					$C_4(E_0,z)$							
0.50	0.608	0.588	0.549	0.491	0.450	0.421	0.398	0.363	0.300	0.269	0.134	0.0715
0.60	0.700	0.662	0.611	0.536	0.478	0.432	0.393	0.332	0.268	0.204	0.129	0.0634
0.70	0.853	0.797	0.726	0.613	0.535	0.460	0.396	0.294	0.222	0.167	0.108	0.0521
0.75	0.976	0.904	0.751	0.562	0.450	0.374	0.318	0.239	0.187	0.147	0.0971	0.0414
0.80	0.434	0.385	0.327	0.259	0.217	0.187	0.164	0.129	0.103	0.0818	0.0514	0.0204
0.85	0.0996	0.0945	0.0876	0.0775	0.0695	0.0631	0.0575	0.0483	0.0383	0.0285	0.0169	0.0052
0.90	0.0100	0.0132	0.0153	0.0161	0.0152	0.0137	0.0122	0.0092	0.0068	0.0048	0.0025	0.0007
1.00	0.0001	0.0003	0.0005	0.0007	0.0007	0.0006	0.0005	0.0003	0.0002	0.0001	0.0001	0.0000

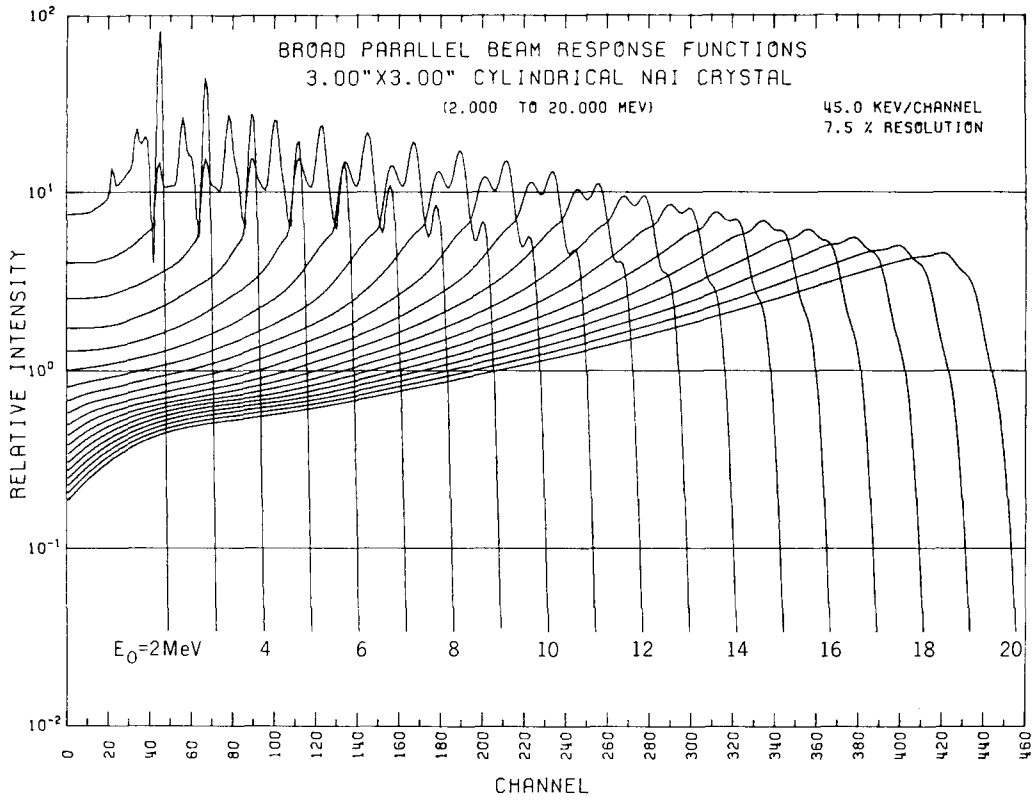

Fig. 9. Set of response functions constructed with use of the data given in tables 6 and 7. Assumed resolution $r(0.661) = 7.5\%$. Curves are normalized so that the area under each is equal to $45\eta(E_0)$. Results pertain to the case of a broad parallel beam incident on the flat endface of a $3'' \times 3''$ detector.

11. Other irradiation geometries

The irradiation geometry can be characterized in terms of the differential flux of gamma rays at the detector site, i.e. the number $n(\theta,\varphi)$ of gamma rays per unit solid angle that cross a unit area of surface perpendicular to the propagation vector $\boldsymbol{u} = (\sin\theta\cos\varphi, \sin\theta\sin\varphi, \cos\theta)$. The angles θ and φ are spherical coordinates in a system whose polar axis coincides with the symmetry axis of the cylindrical detector.

One case of interest is the oblique broad parallel beam, characterized by a differential flux distribution

$$n(\theta,\varphi) = n_0\delta(\cos\theta - \cos\theta_0)\delta(\varphi - \varphi_0), \qquad (10)$$

where n_0 is a normalization constant and δ the delta function. The number of gamma rays entering the detector through one of the flat endfaces is $n_0\pi R^2\cos\theta_0$, that entering through the other endface is zero, and the number entering through the lateral surface is $n_0 2RL\sin\theta_0$, where R and L are the radius and length of the detector.

If the differential flux is isotropic, i.e. with a distribution

$$n(\theta,\varphi) = n_0/4\pi, \qquad (11)$$

one finds, after integrating over all directions of incidence, that the number of gamma rays entering through each flat endface is $n_0\pi R^2/4$, and the number entering through the lateral surface is $n_0\pi RL/2$. Of course one might want to adjust these numbers in order to take into account that one flat endface is usually shielded, at least partially, by the photomultiplier tube, and that the lateral surface may be surrounded by other materials such as anti-coincidence shields.

Another case, which arose in the analysis by Trombka of lunar data from the Apollo 15 mission, is that of a detector with its flat endface pointing toward the surface of the moon. There is a thin layer of radioactive material on the lunar surface due to cosmic-ray bombardment. It is a good approximation to assume that the gamma ray flux from the lunar surface is isotropic over one hemisphere ($0 \leqq \cos\theta \leqq 1$). In this case, which we shall denote as that of a 2π-isotropic flux, the number of gamma rays entering through one of the endfaces is $n_0\pi R^2/4$, that entering through the other endface is zero, and that entering through the lateral surface is $n_0\pi RL/4$.

Taking into account the spherical shape of the lunar

TABLE 8

Detection efficiency $\eta(E_0)$ and peak parameters P_0, P_1 and P_2 of the energy deposition spectrum, for broad parallel beams incident at an angle θ_0 with respect to the detector axis, and for the case of a 2π-isotropic flux. Numbers in parentheses indicate the estimated statistical uncertainty in the last significant figures.

E_0 (MeV)	θ_0	η	P_0	P_1	P_2
0.661	0°	0.877	0.597 (4)		
	60°	0.652	0.578 (7)		
	90°	0.781	0.592 (9)		
	2π-iso.	0.681	0.569 (6)		
6.13	0°	0.622	0.114 (2)	0.119 (2)	0.0447 (12)
	60°	0.423	0.103 (3)	0.114 (3)	0.0482 (24)
	90°	0.522	0.105 (5)	0.115 (5)	0.0490 (31)
	2π-iso.	0.447	0.106 (3)	0.115 (4)	0.0458 (23)
12.0	0°	0.656	0.0425 (11)	0.0720 (15)	0.0248 (9)
	2π-iso.	0.476	0.0375 (20)	0.0642 (26)	0.0261 (17)

surface one can show that gamma rays arriving at the detector site must have obliquity cosines greater than $\cos\theta_{\min}=[1-R_M^2/(R_M+H)^2]^{\frac{1}{2}}$, where R_M (=1738 km) is the radius of the moon and H is the height of the detector above the lunar surface. A typical height in the Apollo 15 experiment was $H=111$ km, corresponding to $\cos\theta_{\min}=0.341$. We note that for $H=0$ one has the limiting case of a 2π-isotropic flux as defined above, and for $H\to\infty$ the limiting case of a broad parallel beam incident perpendicularly. As discussed below, the shapes of the response functions in the two limiting cases are quite close to each other, so that one can dispense with Monte Carlo calculations for intermediate values of H.

We have explored the influence of the irradiation geometry on the response of $3''\times 3''$ detectors at three energies (0.661, 6.13 and 12 MeV). Results of these calculations are given in table 8 for the following circumstances: broad parallel beams incident at angles of 0°, 60° or 90°, and the case of a 2π-isotropic flux as defined above. It can be seen that the peak parameters P_0, P_1 and P_2 of the energy deposition spectrum are nearly independent of the beam geometry. The small observed differences are either within, or not far outside, the limits of the statistical error. When complete response functions are plotted one finds that their shape (but not their normalization) is almost the same in all the cases studied. The normalization factor, i.e. the detection efficiency $\eta(E_0)$, depends more strongly on the irradiation geometry, and can be determined rather simply, without recourse to elaborate Monte Carlo calculations. For convenience we give in table 9 a set of efficiency values for $3''\times 3''$ detectors exposed to a 2π-isotropic flux [obtained with a computer program of Trombka[8])] and compare them with corresponding values for a broad parallel beam incident perpendicularly.

TABLE 9

Detection efficiency $\eta(E_0)$ for a $3''\times 3''$ detector irradiated by a broad parallel beam incident perpendicularly on the endface ($\theta_0=0°$), and for the case of a 2π-isotropic flux.

E_0 (MeV)	$\theta_0=0°$	2π-iso.
0.1	1.000	0.988
0.15	1.000	0.964
0.2	1.000	0.930
0.3	0.988	0.851
0.4	0.956	0.785
0.5	0.924	0.737
0.6	0.894	0.700
0.8	0.843	0.645
1.0	0.802	0.605
1.2	0.768	0.573
1.5	0.728	0.537
2.0	0.684	0.499
3.0	0.641	0.463
4.0	0.624	0.449
5.0	0.620	0.446
6.0	0.621	0.447
8.0	0.629	0.454
10.0	0.643	0.464
12.0	0.656	0.476
15.0	0.675	0.491
20.0	0.702	0.514

We would like to thank Dr. Trombka for encouragement, support and much helpful advice. We are also indebted to Drs. Ferguson and Metzger for putting unpublished data at our disposal, and to Mr. M. J. Silverstein for computational assistance.

References

[1]) J. I. Trombka and R. L. Schmadebeck, Nucl. Instr. and Meth. **62** (1968) 253.

[2]) J. I. Trombka and R. L. Schmadebeck, National Aeronautics and Space Adm. Report NASA SP-3044 (1968).

[3]) I. Adler and J. I. Trombka, *Geochemical exploration of the moon and planets* (Springer, Berlin, 1970).

[4]) J. H. Neiler and P. R. Bell, *Alpha-, beta- and gamma-ray spectroscopy*, vol. 1 (ed. K. Siegbahn; North-Holland Publ. Co., Amsterdam, 1968) p. 245.

[5]) R. van Lieshout, A. H. Wapstra, R. A. Ricci and R. K. Girgis *Alpha-, beta- and gamma-ray spectroscopy*, vol. 1 (ed. K. Sieg bahn; North-Holland Publ. Co., Amsterdam, 1968) p. 501.

[6]) A. Schaarschmidt and H. J. Keller, Nucl. Instr. and Meth. **72** (1968) 82.
[7]) I. Petr, A. Adams and J. B. Birks, Nucl. Instr. and Meth. **95** (1971) 253.
[8]) J. I. Trombka, to be published in Nucl. Instr. and Meth.
[9]) U. Fano, L. V. Spencer and M. J. Berger, *Handbuch der Physik*, vol. 38/2 (Springer, Berlin, 1959) p. 660.
[10]) J. H. Hubbell, Nat. Bur. Std. Publ. NSRDS-NBS 29 (1969).
[11]) M. J. Berger, *Methods in computational physics*, vol. 1 (Academic Press, New York, 1963) p. 135.
[12]) S. Goudsmit and J. L. Saunderson, Phys. Rev. **57** (1940) 24.
[13]) L. Landau, J. Phys. USSR **8** (1944) 201.
[14]) C. Møller, Ann. Physik **14** (1932) 568.
[15]) H. Kolbenstvedt, J. Appl. Phys. **38** (1967) 4785.
[16]) M. J. Berger and S. M. Seltzer, Phys. Rev. C **2** (1970) 621.
[17]) M. J. Berger and S. M. Seltzer, National Aeronautics and Space Adm. Report NASA SP-3012 (1964).
[18]) J. J. Steyn, M. A. Sc. Thesis (University of Toronto, 1951).
[19]) R. L. Heath, U.S. AEC Publ. IDO-16889-1 & 2 (1964).
[20]) G. G. Kelley, P. R. Bell, R. C. Davis and N. H. Lazar, IRE Trans. Nucl. Sci. NS-3 (1956) 57.
[21]) P. Axel, Brookhaven Nat. Lab. Publ. BNL 271 (1953).
[22]) M. P. Fioratti and S. R. Piermattei, Nucl. Instr. and Meth. **96** (1971) 605.
[23]) H. I. Israel, D. W. Lier and E. Storm, Nucl. Instr. and Meth. **91** (1971) 141.
[24]) G. W. Grodstein, Nat. Bur. Std. Circ. no. 583 (1957).
[25]) M. J. Berger and J. Doggett, Nat. Bur. Std. J. Res. **56** (1956) 355; Rev. Sci. Instr. **27** (1956) 269.
[26]) W. F. Miller and W. J. Snow, Rev. Sci. Instr. **31** (1960) 39; Argonne Nat. Lab. Report ANL-6318 (1961).
[27]) L. Jarczyk, H. Knoepfel, J. Lang, R. Müller and W. Wölfli, Nucl. Instr. and Meth. **17** (1962) 310.
[28]) C. T. Schmidt, IRE Trans. Nucl. Sci. NS-7 (1960) 25.
[29]) R. S. Foote and H. W. Koch, Rev. Sci. Instr. **25** (1954) 746.
[30]) M. Giannini, P. R. Oliva and M. C. Ramorino, Nucl. Instr. and Meth. **81** (1970) 104; Comitato Nazionale Energia Nucleare (Rome) Report RT/FI (69) 38 (1969); Comitato Nazionale Energia Nucleare (Rome) Report RT/FI(69)15 (1969).
[31]) E. Nardi, Nucl. Instr. and Meth. **83** (1970) 331.
[32]) J. J. Steyn, R. Huang and D. W. Harris, Trans. Am. Nucl. Soc. **14** (1971) 125.
[33]) C. D. Zerby and H. S. Moran, Oak Ridge Nat. Lab. Report ORNL 2454 (1958).
[34]) C. D. Zerby and H. S. Moran, Nucl. Instr. and Meth. **14** (1962) 115; Oak Ridge Nat. Lab. Report ORNL-3169 (1961).
[35]) C. Weitkamp, Nucl. Instr. and Meth. **23** (1963) 10.
[36]) R. R. Wilson, Phys. Rev. **79** (1950) 204; **84** (1951) 100.
[37]) M. J. Berger, S. M. Seltzer, S. E. Chappell, J. C. Humphreys and J. W. Motz, Nucl. Instr. and Meth. **69** (1969) 181.
[38]) F. Titus, Nucl. Instr. and Meth. **89** (1970) 93.
[39]) A. A. O'Dell, Jr., C. W. Sandifer, R. B. Knowlen and W. D. George, Nucl. Instr. and Meth. **61** (1968) 340.
[40]) H. W. Koch and J. M. Wyckoff, Nat. Bur. Std. J. Res. **56** (1956) 319.
[41]) N. H. Lazar, IRE Trans. Nucl. Sci. NS-5 (1958) 138.
[42]) J. I. Trombka, E. Eller, G. A. Oswald, M. J. Berger and S. M. Seltzer, USAEC Report CONF.-710402, vol. 3 (1971).
[43]) J. Kockum and N. Starfelt, Nucl. Instr. and Meth. **4** (1959) 171.
[44]) R. Hofstadter, E. B. Hughes, W. L. Lakin and I. Sick, Nature **221** (1969) 228.
[45]) E. B. Hughes, R. L. Ford, R. Hofstadter, L. H. O'Neill and J. N. Otis, IEEE Trans. Nucl. Sci. NS-17 (1970) 14.
[46]) R. A. Alvarez, B. L. Berman, R. R. Lasher, T. W. Phillips and S. C. Fultz, Phys. Rev. C **4** (1971) 1673.
[47]) H. Beil, R. Bergère and A. Veyssiere, Nucl. Instr. and Meth. **67** (1969) 293.
[48]) G. W. Clark, G. P. Garmire and W. L. Kraushaar, Astrophys. J. Letters **153** (1968) L203.
[49]) D. A. Kniffen and C. E. Fichtel, Astrophys. J. Letters **161** (1970) L157.
[50]) F. W. Stecker, J. I. Vette and J. I. Trombka, Nature (Phys. Sci.) **231** (1971) 122.
[51]) J. H. Ahlberg, E. N. Nilson and J. L. Walsh, *The theory of splines and their applications* (Academic Press, New York, 1967).